

**Relative humidity and
cirrus cloud
formation**

W. Haag et al.

Freezing thresholds and cirrus cloud formation mechanisms inferred from in situ measurements of relative humidity

W. Haag¹, B. Kärcher¹, J. Ström², A. Minikin¹, U. Lohmann³, J. Ovarlez⁴, and A. Stohl⁵

¹Deutsches Zentrum für Luft- und Raumfahrt (DLR), Institut für Physik der Atmosphäre (IPA), Oberpfaffenhofen, Germany

²Stockholm University, Institute of Applied Environmental Research (ITM), Stockholm, Sweden

³Dalhousie University, Department of Physics and Atmospheric Science, Halifax, Nova Scotia, Canada

⁴Laboratoire de Météorologie Dynamique (LMD) du CNRS, École Polytechnique, Palaiseau, France

⁵Lehrstuhl für Bioklimatologie und Immissionsforschung, Technische Universität München (TUM), Freising, Germany

Received: 24 March 2003 – Accepted: 28 April 2003 – Published: 30 June 2003

Correspondence to: W. Haag (Werner.Haag@dlr.de)

Title Page

Abstract

Introduction

Conclusions

References

Tables

Figures

◀

▶

◀

▶

Back

Close

Full Screen / Esc

Print Version

Interactive Discussion

© EGU 2003

Abstract

Factors controlling the distribution of relative humidity above ice saturation in the upper troposphere and lower stratosphere in the presence of cirrus clouds are examined with the help of microphysical trajectory simulations using a box model. Our findings are related to results from recent field campaigns and global model studies. We suggest that the relative humidities at which ice crystals form in the atmosphere can be inferred from in situ measurements of water vapor and temperature close to, but outside of, cirrus clouds. The comparison with similar measurements performed inside cirrus clouds provides a clue to freezing mechanisms active in cirrus. The comparison with field data reveals distinct interhemispheric differences in cirrus cloud freezing thresholds. Combining the present findings with recent results addressing the frequency distributions of updraft speeds and cirrus ice crystal number densities (Kärcher and Ström, 2003) provides evidence for the existence of complex heterogeneous freezing mechanisms in cirrus, at least in the polluted northern hemisphere, and further emphasizes the key role of gravity wave-induced dynamical variability in vertical air motion at the mesoscale. The key features of distributions of upper tropospheric relative humidity simulated by a global climate model are shown to be in general agreement with both, microphysical simulations and field observations, delineating a feasible method to include and validate ice supersaturation in other large-scale models of the atmosphere, in particular chemistry-transport and weather forecast models.

1. Introduction

Understanding the formation of cirrus clouds in the upper troposphere and tropopause region is a necessary prerequisite in developing the ability to understand and predict the radiative effects of cirrus clouds, their role in precipitation processes and in the hydrological cycle, and hence their impact on climate. High-level ice clouds are thought to freeze-dry air entering the tropical lower stratosphere, thereby influencing the strato-

Relative humidity and cirrus cloud formation

W. Haag et al.

Title Page

Abstract

Introduction

Conclusions

References

Tables

Figures

◀

▶

◀

▶

Back

Close

Full Screen / Esc

Print Version

Interactive Discussion

**Relative humidity and
cirrus cloud
formation**W. Haag et al.

[Title Page](#)[Abstract](#)[Introduction](#)[Conclusions](#)[References](#)[Tables](#)[Figures](#)[◀](#)[▶](#)[◀](#)[▶](#)[Back](#)[Close](#)[Full Screen / Esc](#)[Print Version](#)[Interactive Discussion](#)

© EGU 2003

spheric water vapor (H_2O) budget (Danielsen, 1982; Jensen et al., 1996); modify heating rates in the tropical tropopause region, thereby influencing stratospheric ozone and the stratospheric circulation (Dessler et al., 1996); lead to vertical redistribution of H_2O and freezing nuclei, with a potential to modify the development of supercooled low level clouds (Braham, 1967); and trigger heterogeneous chemistry at middle and high latitudes, thereby possibly contributing to the observed decline of ozone in the midlatitude lower stratosphere (Borrmann et al., 1996).

Despite the recognition of the importance of cirrus clouds, details of their formation mechanisms are not very well understood. In particular, the relative humidities over ice, RHI, at which cirrus ice crystals form (hereafter referred to as freezing thresholds) are difficult to infer from in situ measurements, because the freezing of aerosol particles occurs very rapidly (seconds to minutes) and the thermodynamical variables controlling the phase transition are highly variable over the time scale of cloud formation.

The present work uses information about temperature and specific humidity from atmospheric trajectories in conjunction with a microphysical model (Sect. 2) to simulate frequency distributions of RHI with and without prescribed cirrus cloud formation processes (Sect. 3). In particular, the factors controlling the slopes and cut-offs appearing in the distributions of RHI in ice-supersaturated regions are examined and related to freezing thresholds and freezing mechanisms in cirrus clouds.

Relating the numerical results to field measurements of RHI allows important conclusions to be drawn regarding freezing mechanisms in midlatitude cirrus clouds. By means of global climate model studies we demonstrate that the key features of distributions of RHI in ice-supersaturated regions can be simulated with large-scale models. We thereby expand on previous work mainly on wave clouds proposing a similar methodology (Heymsfield and Miloshevich, 1995; Heymsfield et al., 1998) by using more accurate tools to separate measurements of RHI inside and outside of clouds, by presenting new inferences concerning the dependence of the freezing thresholds on properties of the freezing aerosol, by highlighting interhemispheric differences between freezing mechanisms in cirrus, and by delineating the treatment of ice supersaturation

in global atmospheric models.

2. Methodology

2.1. Distributions of relative humidity

A growing body of in situ observations shows that the upper troposphere and tropopause region at low and middle latitudes are frequently supersaturated with respect to ice (Jensen et al., 2001), allowing the formation and persistence of cirrus clouds and aircraft contrails. The occurrence of cirrus clouds extending well into the lower stratosphere in the wintertime polar regions is a well known phenomenon (Kärcher and Solomon, 1999). Recent satellite data provide supporting evidence for the widespread existence of subvisible cirrus at the tropopause (Spang et al., 2002).

Observations suggest that the distribution of RHI in ice supersaturated regions follows an almost exponential decay, indicating that the underlying processes that cause this functional dependence act in a statistically independent manner (Gierens et al., 1999). The question arises of how realistic probability distributions of RHI can be generated with the help of a model to be studied systematically.

We suggest that such distributions are primarily brought about by vertical air motions that cause a certain distribution of atmospheric temperatures T . Variability of H_2O also plays a role, but is less influential. When distributions of T and H_2O concentrations are combined to derive RHI, the resulting distributions of RHI exhibit a quasi-exponential decrease towards high RHI values, in agreement with observations. A more detailed investigation of these basic features will be presented in a separate study.

In the present study, we compute fields of RHI by advecting H_2O along domain-filling atmospheric trajectories and allowing ice formation and evaporation, that is, the formation and disappearance of cirrus clouds. We focus on cold cirrus that form directly from freezing aerosol particles. Different freezing thresholds of one type of chemically uniform aerosols are imposed in the model to investigate their impact on the distributions

Relative humidity and cirrus cloud formation

W. Haag et al.

Title Page

Abstract

Introduction

Conclusions

References

Tables

Figures

◀

▶

◀

▶

Back

Close

Full Screen / Esc

Print Version

Interactive Discussion

**Relative humidity and
cirrus cloud
formation**W. Haag et al.

[Title Page](#)[Abstract](#)[Introduction](#)[Conclusions](#)[References](#)[Tables](#)[Figures](#)[◀](#)[▶](#)[◀](#)[▶](#)[Back](#)[Close](#)[Full Screen / Esc](#)[Print Version](#)[Interactive Discussion](#)

© EGU 2003

of RHI. The initial H₂O mixing ratio on each trajectory (representing the source region of H₂O) is kept fixed, and RHI varies according to changes of T , air pressure p , and the calculated rates of H₂O deposition onto and evaporation from aerosol and cirrus ice particles.

5 The trajectories follow the motions caused by buoyancy waves with wavelengths sufficiently long to be resolved by the ECMWF model. However, smaller-scale gravity waves, non-hydrostatic waves, and deep convection are not explicitly resolved. The trajectories reflect these processes only to the extent that the physical parameterizations feed back on the grid-scale winds, generally underestimating small-scale temperature variability along the trajectories (Kärcher and Ström, 2003).

10 Our approach to study distributions of RHI is consistent with the work of Gettelman et al. (2000). These authors have employed a global tracer model to simulate the distribution of H₂O in the upper troposphere and lower stratosphere. Distributions of H₂O observed by satellites and radiosondes could be qualitatively reproduced by just including large scale advection of H₂O along with the restriction that the air be at or below ice saturation. While this method cannot predict ice supersaturation, it suggests that cirrus cloud formation associated with vertical motions is of primary importance in simulating upper tropospheric and lower stratospheric H₂O, a fact studied in detail below.

20 2.2. Trajectories and microphysical simulations

We combine the microphysical aerosol/cirrus model APSC (Advanced Particle Simulation Code) developed at Deutsches Zentrum für Luft- und Raumfahrt (DLR) with three-dimensional trajectories derived from high-resolution wind fields taken from the European Centre for Medium-Range Weather Forecasts (ECMWF) with the help of the kinematic trajectory model FLEXTRA developed at the Technical University of Munich (Stohl and Seibert, 1998).

The trajectory calculations were driven with operational ECMWF data. In November 2001, the ECMWF operational forecast model had a spectral truncation of T511 (equiv-

**Relative humidity and
cirrus cloud
formation**W. Haag et al.

[Title Page](#)[Abstract](#)[Introduction](#)[Conclusions](#)[References](#)[Tables](#)[Figures](#)[◀](#)[▶](#)[◀](#)[▶](#)[Back](#)[Close](#)[Full Screen / Esc](#)[Print Version](#)[Interactive Discussion](#)

© EGU 2003

alent to ~ 40 km horizontal resolution) and 60 vertical levels. We retrieved the ECMWF data on a global latitude/longitude grid of 1° resolution and on a higher-resolution (0.5°) nest covering most of the main area of interest (120°W – 30°E , 18°N – 66°N). Analyses were used every 6 h (00:00, 06:00, 12:00, 18:00 UTC) and 3-hour shifted forecasts (at 03:00, 09:00, 15:00, 21:00 UTC) in order to achieve the maximum temporal resolution available from ECMWF. The FLEXTRA trajectory model uses bicubic horizontal, quadratic vertical, and linear time interpolation. Fully three-dimensional trajectories were calculated and, thus, no isentropic assumption was invoked.

Fourteen day backward trajectories were started every 30 hPa between 150 hPa and 450 hPa from a regular grid (1° latitude and longitude), covering the region 120°W – 30°E , 25°N – 65°N . Trajectories were started on 28 November 2001 at 18 UTC, and trajectory positions, pressure, specific humidity and other information were stored every hour. Intermediate trajectory temperature and pressure values were obtained by linear interpolation in time of the FLEXTRA results.

The microphysical simulations were carried out as described by Haag et al. (2003). Freezing and growth processes of aerosol and ice particles were treated using a scheme that exactly conserves the total mass of H_2O present in the gas and particle phase along a given trajectory, without making equilibrium assumptions. Only water vapor was allowed to interact with the particle phase. The aerosol size distribution was lognormal, with a total number density of 390 cm^{-3} , a mean mass diameter (dry particles) of 100 nm, and a geometric standard deviation of 1.8. The aerosol particles were either composed of H_2O and sulfuric acid (H_2SO_4) that freeze homogeneously according to an activity-based parameterization of nucleation rates (Koop et al., 2000), or represented some type of ice nuclei with a prescribed (nominal) heterogeneous freezing threshold of 130 %. To calculate heterogeneous nucleation rates, we applied the shifted-activity method described elsewhere (Kärcher and Lohmann, 2003). The saturation vapor pressure over ice was taken from Marti and Mauersberger (1993).

The nominal heterogeneous threshold is defined such that one particle with a radius of $0.25\ \mu\text{m}$ freezes in one second at a relative humidity over ice of 130 %. In the model,

**Relative humidity and
cirrus cloud
formation**W. Haag et al.

[Title Page](#)[Abstract](#)[Introduction](#)[Conclusions](#)[References](#)[Tables](#)[Figures](#)[◀](#)[▶](#)[◀](#)[▶](#)[Back](#)[Close](#)[Full Screen / Esc](#)[Print Version](#)[Interactive Discussion](#)

© EGU 2003

depending on the cooling rates at the point of ice formation, particles with very different sizes may contribute to cirrus formation. Therefore we expect a range of freezing thresholds as in the homogeneous case, where the freezing thresholds additionally depend on T .

5 When no cirrus clouds are present along a trajectory, we used a constant time step Δt of 120 s to advance the calculations. If RHI exceeded 125 %, Δt was decreased to 2 s. Around the time of freezing, we set $\Delta t = 0.25$ s in order to simulate the freezing processes precisely. After the formation phase, we used a constant time step of 20 s as long as cirrus clouds are present. The variable time steps ensured that the simu-
10 lations were fast, as we ran the APSC along thousands of trajectories, and accurate, as required to correctly resolve details of water uptake and freezing.

Along each trajectory, we stored the RHI and other microphysical information every 120 s to mimick a uniform sampling of data points, which is required to avoid statistical aberrations in the resulting frequency distributions. This requirement is not necessarily
15 met in field measurements, but can easily be accounted for in the present type of calculations. Data points with a total ice particle number density $n_i < 10^{-3} \text{ cm}^{-3}$ were considered as out-of-cloud data points.

A typical result from a combined FLEXTRA/APSC simulation including cirrus formation by homogeneous freezing is depicted in Fig. 1. In the first cloud event at day 3,
20 about 0.03 ice crystals form per cm^3 of air in a moderate cooling event near 235 K. The peak RHI reach almost 150 % during cloud formation and then RHI drops to values near saturation for most of the cloud lifetime. The cloud evaporates at the end of day 5 because the air mass descends. The trajectory rises again very rapidly on day 12 and produces a second cirrus cloud, containing about 0.8 ice crystals per cm^3 of air;
25 this time the cooling rate is much faster than during the first cloud event and the cloud lifetime is shorter.

The fact that initial H_2O mixing ratios are fixed for two weeks along each trajectory and that sedimentation of large ice crystals is neglected possibly leads to an overestimation of cirrus occurrence and lifetime because too much H_2O is transported to high

altitudes. On the other hand, we cannot reinitialize the APSC with the ECMWF specific humidities every time the ECMWF provides updated values, because ice supersaturation is not allowed to occur in the ECMWF model and we would not be able to nucleate cirrus above ice saturation in the APSC. In any case, this issue does not affect the basic conclusions of this work, but should be accounted for in more detailed analyses of cirrus cloud properties with the present methodology.

3. Results and discussion

In what follows, we work out the main features of the RHI distribution and study their link to freezing processes in cirrus (Sect. 3.1). The basic results do not depend on the choice of the trajectory space and time domain or on details of the cirrus cloud microphysics. To provide a link to observations and global simulations, we relate our findings to the INCA (Interhemispheric Differences in Cirrus Properties From Anthropogenic Emissions) field experiment (Sect. 3.2) and to simulations of RHI carried out with the general circulation model (GCM) ECHAM (Sect. 3.3).

3.1. Connecting relative humidity and cirrus formation

The black distribution $f(\text{RHI})$ shown in Fig. 2 results from the statistical evaluation of RHI using all (a total of 66,440) trajectories. The only process affecting RHI was atmospheric transport, cirrus formation was not included in these calculations. The blue and red distributions represent subsets characterized by a net upward (541 trajectories) and net downward (838 trajectories) motion, respectively. The criterion applied to select these subsets was that the starting points and endpoints (after two weeks) of each trajectory exhibit a net vertical displacement of at least 200 hPa. Trajectories from the upward subset ended between 150 hPa and 210 hPa, those from the downward subset ended between 390 hPa and 450 hPa.

In the case of net upward air motion, cooling of air parcels with relatively high H_2O

Relative humidity and cirrus cloud formation

W. Haag et al.

Title Page

Abstract

Introduction

Conclusions

References

Tables

Figures

⏪

⏩

◀

▶

Back

Close

Full Screen / Esc

Print Version

Interactive Discussion

mixing ratios from lower tropospheric levels generates high RHI values. On the other hand, sinking air parcels originating near the tropopause contain much less H_2O and become even dryer when T increases, strongly reducing the frequency of occurrence of high ice supersaturations.

5 All curves fall off above ice saturation. The downward moving trajectories fall off most rapidly with a well defined slope already in strongly subsaturated air (starting at about 50 % RHI). The slope of $f(\text{RHI})$ decreases when going from net downward to net upward motion, emphasizing the importance of updrafts in creating supersaturation. The fact that the black and blue distributions have similar slopes indicates that the probability to find a given supersaturation with respect to ice is primarily determined by
10 the upward moving trajectories.

To study the impact of cirrus cloud formation on the RHI distributions, we now discuss combined FLEXTRA/APSC simulations, the results of which are shown in Fig. 3. We have performed two different types of simulations. In the first type, labelled HOM, growth and homogeneous freezing of supercooled $\text{H}_2\text{SO}_4/\text{H}_2\text{O}$ aerosols is considered. In the second type, labelled HET, we consider heterogeneous freezing of the same aerosol size spectrum at a prescribed freezing threshold value of 130 %, mimicking cloud formation by efficient ice nuclei. (The heterogeneous freezing threshold could lie anywhere between 100 % and the water saturation limit; this specific choice
20 is motivated by the field experiments discussed in Sect. 3.2.) To be able to perform the calculations in a reasonable time frame, we reduced the number of trajectories by a factor of 20 and ran APSC on 3,320 selected trajectories. Also, we have evaluated $f(\text{RHI})$ without cloud formation, labelled ADV, to compare with the results including cirrus. In all cases, data points with relative humidities above water saturation and temperatures
25 above 235 K have been removed from the statistics, essentially reducing the analysis to vertical levels between 150 hPa and ~ 300 hPa.

The pure transport case ADV is similar to the black distribution shown in Fig. 2. The most obvious change of $f(\text{RHI})$ introduced by cirrus cloud formation compared to case ADV is the appearance of a cut-off in the supersaturated region. In case HOM (HET),

Relative humidity and cirrus cloud formation

W. Haag et al.

[Title Page](#)[Abstract](#)[Introduction](#)[Conclusions](#)[References](#)[Tables](#)[Figures](#)[◀](#)[▶](#)[◀](#)[▶](#)[Back](#)[Close](#)[Full Screen / Esc](#)[Print Version](#)[Interactive Discussion](#)

**Relative humidity and
cirrus cloud
formation**W. Haag et al.

[Title Page](#)[Abstract](#)[Introduction](#)[Conclusions](#)[References](#)[Tables](#)[Figures](#)[◀](#)[▶](#)[◀](#)[▶](#)[Back](#)[Close](#)[Full Screen / Esc](#)[Print Version](#)[Interactive Discussion](#)

© EGU 2003

no data points above $\sim 158\%$ ($\sim 136\%$) are found outside of clouds, as indicated by the arrows in Fig. 3. At the time of cloud onset, when n_j increases above 10^{-3} cm^{-3} , we calculate the median freezing thresholds RHI_m that are smaller than the cut-offs and are plotted as circles with error bars, see below. (In fact, the cut-offs are equal to the 100 %-percentiles.) In case HOM (HET), we obtain $\text{RHI}_m = 151\%$ ($\text{RHI}_m = 129\%$); as expected, the blue and red curves show a rather sharp decrease around RHI_m .

Our simulations show that the cut-off of the RHI distributions in ice-supersaturated regions is directly related to the onset of freezing in cirrus clouds. This of course requires that the underlying temperatures exhibit enough variability to generate RHI values higher than the freezing thresholds if no cirrus would form; this requirement is fulfilled, see black curve in Fig. 3.

The median values are averages over all individual ice formation events, involving different cooling rates and therefore different portions of the freezing particle size distribution. In case HET, the value $\text{RHI}_m = 129\%$ is near the prescribed threshold of 130 % to calculate the freezing rate. The same holds for case HOM, where in addition, the freezing thresholds also depend on T (Koop et al., 2000). (The calculated median homogeneous freezing temperature is 216.5 K.) The error bars around the median values show the values of the first and third quartiles, indicating the rather small variance of RHI_m . Careful inspection reveals that the variance in case HOM is slightly larger than in case HET and is brought about by the additional T -dependence of the freezing thresholds in case HOM.

We have argued above that the slope of $f(\text{RHI})$ is determined by the transport properties of the trajectories. How does the decrease of the slopes between the three different cases in Fig. 3 come about, although the very same trajectories have been used in all cases? As we sample out-of-cloud points to determine $f(\text{RHI})$, the cirrus clouds themselves cannot alter the properties of the distributions between 100 % and the cut-off. However, cirrus formation and persistence indirectly affects the slope of $f(\text{RHI})$. In case HOM, all data points above 158 % are turned from out-of-cloud into inside cloud data points. They are considered in case ADV, but no longer in the HOM data set. As the

**Relative humidity and
cirrus cloud
formation**W. Haag et al.

[Title Page](#)[Abstract](#)[Introduction](#)[Conclusions](#)[References](#)[Tables](#)[Figures](#)[◀](#)[▶](#)[◀](#)[▶](#)[Back](#)[Close](#)[Full Screen / Esc](#)[Print Version](#)[Interactive Discussion](#)

© EGU 2003

neglected data points belong to trajectories that primarily produce large supersaturations and eventually lead to cloud nucleation, the slope increases when homogeneous freezing is considered. The same selection effect further increases the slope in case HET, as even more such data points along cloud-forming trajectories (all above 136 %) are excluded from the statistical analysis.

We note that the changes of the f (RHI) slopes caused by the different assumptions for aerosol freezing (compare the slopes of blue and red distributions in Fig. 3) appear to be somewhat smaller compared with the changes caused by the dynamical properties of the trajectories (compare the slopes of blue and red distributions in Fig. 2). The fact that transport, and possibly to a lesser degree cloud formation, determines the probability to find ice-supersaturated regions renders a quantitative comparison of the slopes of modeled and measured RHI distributions difficult, unless the meteorological wind fields and physical relations governing cirrus formation, growth, and persistence are well captured by models. We come back to this point in Sects. 3.2.1 and 3.3.

3.2. Observations

Two field campaigns were performed during INCA, one in the midlatitude southern hemisphere (SH) out of Punta Arenas, Chile, one in the midlatitude northern hemisphere (NH) out of Prestwick, Scotland, under comparable meteorological conditions. Water vapor mixing ratios were measured in situ by a frost-point hygrometer and these measurements were converted into RHI using the measured air temperature and pressure. Details of these measurements are discussed elsewhere (Ovarlez et al., 2002); the absolute uncertainty of RHI is 3% (one standard deviation, 1σ). The existence of RHI values outside the 3σ -limits ($\pm 9\%$) is extremely unlikely. The increase in RHI due to evaporation of small (diameter $1\ \mu\text{m}$) ice crystals or water-rich aerosol particles in the air inlet is estimated to be well below 1%.

3.2.1. Freezing threshold relative humidities

The original data are archived at 1 Hz time resolution in the INCA data base. We excluded all data points above water saturation and above 235 K to focus on cold cirrus that form by freezing of aerosol particles, as in the model analysis presented in Sect. 3.1. Our criterion to distinguish between data points inside and outside of cirrus clouds was more conservative than the one based on cloud extinction used by Ovarlez et al. (2002). Here we define a data point as being outside of clouds when the ice particle number density n_i measured by the Counterflow Virtual Impactor (CVI) was below 0.01 cm^{-3} . As the CVI is sensitive to even smaller values of n_i , we have checked that the resulting $f(\text{RHI})$ did not change when using $n_i < 0.001 \text{ cm}^{-3}$ (which corresponds to the criterion used in the APSC to sort out the out-of-cloud data points), but the resulting smaller amount of data left with these criteria increased the statistical error.

The hygrometer has a response time of ~ 4 s. We have checked that the distributions shown in Fig. 4 do not significantly change when we applied the criterion $n_i < 0.01 \text{ cm}^{-3}$ for 4 consecutive seconds. Further, the $f(\text{RHI})$ remain similar when 4 s-means of RHI are calculated, or when 4 s-means of T , p , and H_2O mixing ratio are calculated and RHI is derived from these values. We have binned the data into 4 % intervals to roughly account for the experimental uncertainty. The use of 2 % and 8 % intervals just leads to more or less data smoothing compared to 4 % intervals, leaving slopes and locations of the cut-offs almost unchanged.

The resulting distributions are shown in Fig. 4. A comparison with the modeled distributions (Fig. 3) shows an excellent agreement between the location of the cut-offs (rightmost RHI data points). Recall that in the model, the cut-offs appear at 136 % (HET) and 158 % (HOM), marked with arrows in Fig. 4. In the observations with RHI data binned into 4 % intervals, they lie in the range 134–138 % (NH) and 158–162 % (SH).

In the model, we assume homogeneous freezing as the underlying cirrus formation mechanism, which seems to be appropriate to describe the onset of freezing in the SH

Title Page

Abstract

Introduction

Conclusions

References

Tables

Figures

◀

▶

◀

▶

Back

Close

Full Screen / Esc

Print Version

Interactive Discussion

**Relative humidity and
cirrus cloud
formation**W. Haag et al.

[Title Page](#)[Abstract](#)[Introduction](#)[Conclusions](#)[References](#)[Tables](#)[Figures](#)[⏪](#)[⏩](#)[◀](#)[▶](#)[Back](#)[Close](#)[Full Screen / Esc](#)[Print Version](#)[Interactive Discussion](#)

© EGU 2003

data set. The heterogeneous freezing mechanism assumed in the other model study nicely explains the observed, significantly lower cut-off in the NH data set. The NH data cannot be explained by homogeneous freezing of solution droplets at temperatures below 235 K, as cut-off RHI values outside the 3σ -limits $136 \pm 9\%$ (NH) and $160 \pm 9\%$ (SH) are extremely unlikely. We will add more inferences for freezing mechanisms in Sect. 3.2.2.

While we cannot compare the slopes of the calculated and observed distributions quantitatively as explained at the end of Sect. 3.1, we find another remarkable agreement between model and measurements with regard to the relative difference in the slopes. In both cases, the slope of the NH data (case HET) is steeper than the slope of the SH data (case HOM). This strongly increases confidence in our proposed interpretation of RHI cut-offs taken outside of cirrus clouds with respect to freezing thresholds.

One may argue that the difference in freezing thresholds observed during the INCA campaigns is brought about by a difference in the minimum temperatures between the campaigns, rather than by differences in the freezing properties of aerosols. The overall temperature distributions during INCA were relatively similar, with mean values of 224.7 K (SH) and 226.2 K (NH). The minimum temperature was near 210 K (SH) and 216 K (NH), but the probability to measure such low values was very low. We have checked that the minimum temperatures were low enough and the observed temperature distributions had sufficient variability to produce RHI values above the respective freezing thresholds.

Aerosol sources were variable during the NH campaign; thus one may further argue that the apparent freezing threshold of $\sim 130\%$ in the NH is caused by a combination of ice nuclei that started freezing very early (near 100%) and very late (near the homogeneous limit), i.e., not all aerosol particles initiated freezing around 130% are assumed here. With the help of Fig. 5 we demonstrate that the apparent threshold of 130% was unlikely to be caused by particles with very different freezing properties.

In Fig. 5, the black distribution is the same as plotted in Fig. 4 for the NH measurements. Additionally, we show distributions computed with a subset of the data, repre-

**Relative humidity and
cirrus cloud
formation**W. Haag et al.

[Title Page](#)[Abstract](#)[Introduction](#)[Conclusions](#)[References](#)[Tables](#)[Figures](#)[◀](#)[▶](#)[◀](#)[▶](#)[Back](#)[Close](#)[Full Screen / Esc](#)[Print Version](#)[Interactive Discussion](#)

© EGU 2003

5 sending measurements in clean (dotted curve) and polluted air masses (solid curve). The distinction between clean and polluted cases has been made on the basis of measured concentrations of condensation nuclei (CN) larger than 14 nm in diameter. Approximately 30 % of the NH data are associated with low ($< 170 \text{ cm}^{-3}$) and high ($> 400 \text{ cm}^{-3}$) ambient CN concentrations. We note in passing that the clean NH cases are similar to the average SH data in terms of CN concentrations (Minikin et al., 2003).

10 The three distributions shown in Fig. 5 are almost identical within the range of experimental uncertainty, although they represent conditions with markedly different CN number densities. The total number of CN likely contains all of the freezing particles, but may overemphasize the contribution of particles that did not freeze (typically more than 90 % of the total). Therefore, we have also analyzed other data subsets, namely accumulation mode particles with diameters above 100 nm and nonvolatile, refractory particles (presumably black carbon) with diameters above 10 nm, and have classified them into clean and polluted cases. The respective number densities were $< 10 \text{ cm}^{-3}$ (accumulation mode) and $< 10 \text{ cm}^{-3}$ (nonvolatile) in the clean cases and $> 20 \text{ cm}^{-3}$ (accumulation mode) and $> 40 \text{ cm}^{-3}$ (nonvolatile) in the polluted cases. The results we have obtained are almost identical to those presented in Fig. 5 and are therefore not shown.

20 Taken together, this finding has two implications: first, the apparent threshold of 130 % was likely caused by particles with similar freezing thresholds, almost independent of their source region, suggesting that even the NH background aerosol exhibits signatures of pollution (expressed here as freezing below the homogeneous limit). Second, none of the detected differences in aerosol particle concentrations (total CN, accumulation mode, total nonvolatile) between the NH and SH (Minikin et al., 2003) are responsible for the differences seen in the distributions of RHI between the two hemispheres. It is therefore highly likely that differences in chemical or morphological particle properties have caused the difference in freezing thresholds as given in Fig. 4. We get back to this point towards the end of Sect. 3.2.2.

3.2.2. Freezing mechanisms

We do not discuss the overall distributions of RHI inside cirrus and refer to Ovarlez et al. (2002) for more details. Instead, we focus on the in-cloud distributions above ice saturation and compare them with the measurements taken outside of cirrus, with particular emphasis on the cut-off values. The modeled in-cloud distributions are complementary to the out-of-cloud distributions in the sense that data points along the trajectories with $n_i > 10^{-3} \text{ cm}^{-3}$ were considered as in-cloud data points (Sect. 2.2). In generating the INCA distributions, we define data points as being inside clouds when the CVI detects at least 10^{-2} cm^{-3} ice particles, complementary to the out-of-cloud statistics (Sect. 3.2.1).

The resulting distributions of RHI inside of cirrus clouds is shown in Fig. 6. As for the out-of-cloud discussion, we have binned the distributions into 4 % intervals. In the SH data set, the cut-off lies in the range 162–166 %. In the NH data set, the cut-off lies between 158–162 %. These values are now compared to those shown in Fig. 4.

We first discuss the SH measurements. The mean cut-off ~ 164 % found inside clouds is a few percent above the mean cut-off ~ 160 % found outside of clouds. This is within the experimental uncertainty, and consistent with the APSC results. In the model, the cut-off inside cirrus is ~ 159 % (not shown), about 1 % larger than the cut-off outside of clouds. It is known that low temperatures and high cooling rates increase the difference between the onset RHI (only detectable outside of clouds) and the peak RHI (only detectable inside clouds) during freezing events. For example, at $\sim 213 \text{ K}$ and a cooling rate of 0.9 K min^{-1} , the difference ΔRHI is about 2 % in the simulations reported by Haag et al. (2003).

The difference is caused by a kinetic limitation active during freezing: the nascent ice particles reduce the saturation and shut off nucleation only after a certain time scale that increases when T is lowered. This increases the peak RHI, and the difference ΔRHI increases with decreasing T (Haag et al., 2003). If the observed difference $\Delta \text{RHI} \simeq 4$ % was statistically significant, the above discussion would provide a consis-

Title Page

Abstract

Introduction

Conclusions

References

Tables

Figures

◀

▶

◀

▶

Back

Close

Full Screen / Esc

Print Version

Interactive Discussion

**Relative humidity and
cirrus cloud
formation**W. Haag et al.

[Title Page](#)[Abstract](#)[Introduction](#)[Conclusions](#)[References](#)[Tables](#)[Figures](#)[◀](#)[▶](#)[◀](#)[▶](#)[Back](#)[Close](#)[Full Screen / Esc](#)[Print Version](#)[Interactive Discussion](#)

© EGU 2003

tent explanation when homogeneous freezing is assumed to be the dominant path to cirrus formation. However, the experimental uncertainty of RHI of $\pm 3\%$ (1σ -limits) does not permit to draw a definite conclusion.

The situation is completely different in the NH measurements. The mean cut-off $\sim 162\%$ found inside clouds is significantly above the mean cut-off $\sim 134\%$ found outside of clouds. This marked difference cannot be explained by experimental uncertainty (recall the 3σ -limits of $\pm 9\%$), and is not consistent with the APSC results. In the model, the cut-off inside cirrus is $\sim 138\%$ (not shown), only about 2% larger than the cut-off outside of clouds. This difference is similar to the homogeneous case. We argue that the model assumption regarding the heterogeneous freezing mechanism (pure heterogeneous nucleation of ice in a single type of aerosols) is incorrect.

We propose the following hypothesis, consistent with the INCA observations. In the NH, freezing was initiated by a limited number of efficient ice nuclei that trigger ice formation well below the homogeneous limit, at an RHI value near 130% . This explains why the cut-off RHs measured outside of clouds were near 130% (see Figs. 4 and 5). However, the vertical wind speeds prevailing during the campaign were high enough on average to frequently activate homogeneous nucleation in the much more abundant supercooled aerosol particles, in addition to the few ice nuclei. This explains why the cut-off RHs measured inside clouds were near the homogeneous limit.

The analyses of frequency distributions of updraft speeds and ice crystal number densities measured during INCA strongly support this hypothesis (Kärcher and Ström, 2003). The SH and NH distributions were found to be remarkably similar when the NH data set was cleared of convective influence (which was absent in the SH). The mean updraft speed was $\sim 25\text{ cm s}^{-1}$ in both cases. A primary concentration peak within $0.1 - 10\text{ cm}^{-3}$ occurs in both data sets, with almost identical mean values $1.2 - 1.4\text{ cm}^{-3}$, presumably caused by gravity wave-driven homogeneous nucleation. Differences in the low concentration region ($< 0.1\text{ cm}^{-3}$) could be explained in part by heterogeneous freezing processes caused by a limited number of ice nuclei.

Heterogeneous ice nuclei could suppress homogeneous nucleation and substan-

**Relative humidity and
cirrus cloud
formation**W. Haag et al.

[Title Page](#)[Abstract](#)[Introduction](#)[Conclusions](#)[References](#)[Tables](#)[Figures](#)[◀](#)[▶](#)[◀](#)[▶](#)[Back](#)[Close](#)[Full Screen / Esc](#)[Print Version](#)[Interactive Discussion](#)

© EGU 2003

tially lower the number of ice crystals formed compared to pure homogeneous nucleation (Kärcher and Lohmann, 2003), under three assumptions: (i) ice nuclei must be present in addition to liquid aerosol particles, and both types of particles are, at least to some degree, externally mixed; (ii) the updraft speed stays constant during the freezing event; (iii) the peak number of ice nuclei present must not exceed a critical value, this value depending on the freezing threshold of the ice nuclei, on temperature, and on the vertical wind speed in rising air parcels. A notable difference between NH and SH mean ice crystal number densities and updraft speeds was not observed (see above). This implies that (i) the updraft speeds associated with small-scale waves were sufficiently high to always activate the homogeneous mode and/or (ii) liquid aerosols and ice nuclei were internally mixed.

Recent analyses of residual particles evaporated from the cirrus ice crystals measured during INCA (Seifert et al., 2002) suggests that the size distribution of particles involved in cirrus nucleation could not be explained by pure homogeneous freezing, supporting the crucial role of size-dependent aerosol chemistry in determining the freezing properties of aerosol particles inferred from Fig. 5. As this result was found for both, the NH and SH measurements, this implies that the heterogeneous ice nuclei present in the SH had freezing thresholds very close to the homogeneous limits. In this case, they would alter the residual particle size distribution, but would not affect the cut-off and peak relative humidities, as shown in Figs. 4 and 6, respectively.

Further detailed studies, constrained by the combination of results from this work, the residual particle analyses (Seifert et al., 2002), and the updraft speed and ice crystal concentration analyses (Kärcher and Ström, 2003), are necessary to consolidate our hypothesis and to corroborate our inferences about the freezing mechanisms in cirrus clouds prevailing during the INCA measurements.

3.3. GCM results

Most global models of the atmosphere that include high-level cirrus clouds apply the saturation adjustment scheme. In this scheme, excess ice supersaturation created

**Relative humidity and
cirrus cloud
formation**W. Haag et al.

[Title Page](#)[Abstract](#)[Introduction](#)[Conclusions](#)[References](#)[Tables](#)[Figures](#)[◀](#)[▶](#)[◀](#)[▶](#)[Back](#)[Close](#)[Full Screen / Esc](#)[Print Version](#)[Interactive Discussion](#)

© EGU 2003

during a time step is transferred to cloud ice. Therefore, supersaturation with respect to ice is not allowed to occur in these models. Only recently, the adjustment scheme could be abandoned with the help of a novel parameterization of cirrus cloud formation. This allowed to calculate probability distributions of RHI in ice supersaturated regions along with cirrus clouds formed by homogeneous freezing of supercooled aerosols in a GCM (Lohmann and Kärcher, 2002).

The ECHAM version used here differs from the one previously used for the comparison with relative humidity data from the MOZAIC (Measurement of Ozone on Airbus In-service Aircraft) project. The main change relevant to our study is that the number of hygroscopic aerosols that is present in the upper troposphere has been increased by assuming newer observed aerosol size distributions and increasing the minimum number density of aerosol particles assumed to always be present from 1 to 10 cm⁻³, in better accordance with observations (Minikin et al., 2003). For a more detailed description, see Lohmann et al. (2003); differently from what has been described in Lohmann et al. (2003), the advection of cloud droplet and ice crystal number concentrations is now formulated in terms of number of particles per unit mass of air rather than per unit volume of air.

The updraft velocity w needed for ice crystal formation is given as the sum of the grid mean vertical velocity \bar{w} and a turbulent contribution Δw obtained from the turbulent kinetic energy (Lohmann and Kärcher, 2002): $w = \bar{w} + c\Delta w$, where c is a tuning parameter. We have shown that this simple approach provides a reasonable estimate for the number density of cirrus ice crystals averaged over a grid box, assuming homogeneous freezing as the dominant pathway to nucleate the cloud particles, but is unable to reproduce cloud microphysical parameters in more detail (Kärcher and Ström, 2003).

In the reference simulation SEMIL discussed below, we use the semi-Lagrangian transport scheme developed by Rasch and Williamson (1990). No semi-Lagrangian scheme is per se mass conserving due to the interpolation of the Lagrangian departure points onto a regular grid at every time step. Therefore the masses of water vapor, cloud water, and the aerosol mass mixing ratios are conserved by employing a mass

**Relative humidity and
cirrus cloud
formation**W. Haag et al.

[Title Page](#)[Abstract](#)[Introduction](#)[Conclusions](#)[References](#)[Tables](#)[Figures](#)[◀](#)[▶](#)[◀](#)[▶](#)[Back](#)[Close](#)[Full Screen / Esc](#)[Print Version](#)[Interactive Discussion](#)

© EGU 2003

fixer. Rasch and Lawrence (1998) developed an improved transport scheme (Spitfire) by introducing a separate mass continuity equation and casting it in flux form. Thus, it now conserves tracer mass and is almost monotonic. It is used in the simulations SPITF and SPITF-HIGHW. SPITF-HIGHW assumes a higher contribution from the turbulent kinetic energy ($c = 1.33$) as is used for cloud droplet formation.

Figure 7 depicts distributions of RHI derived from data taken on commercial aircraft (MOZAIC) mainly over the North Atlantic region (Gierens et al., 1999), along with f (RHI) derived from ECHAM simulations in the same location, assuming homogeneous freezing as the only path to form cirrus clouds. In ECHAM, we used the semi-Lagrangian advective transport scheme (SEMIL) and the superior transport scheme (SPITF). These two simulations have been carried out with $c = 0.7$ to calculate vertical wind speeds. The simulation SPITF-HIGHW assumes a subgrid-scale turbulent contribution about twice as large ($c = 1.33$), leading to more frequent cloud formation events and a larger mean number of ice crystals.

We first focus attention to the left panel, showing data around the 200 hPa level. Compared to case SEMIL, the use of the superior transport scheme slightly lowers the probability to find high ($> 120\%$) RHI, keeping the lower values almost unchanged, see case SPITF. This supports our conclusion drawn from the trajectory simulations that the slope of f (RHI) is sensitive to changes of atmospheric transport properties.

Increasing the vertical wind speeds, however, significantly reduces the overall probability to find ice supersaturated regions, keeping the slope almost unchanged, compare SPITF with SPITF-HIGHW. While more clouds with higher average crystal concentrations form in case SPITF-HIGHW, the cut-off remains unchanged as we have not altered the underlying homogeneous freezing mechanism. This supports another conclusion from above, namely that the impact of cloud formation on the slopes of f (RHI) above ice saturation is smaller than the impact of changes in transport properties.

Generally, the slopes of the SPITF and SPITF-HIGHW cases agree well with the MOZAIC data. According to the discussions above, we cannot expect a perfect agreement, inasmuch the meteorological conditions that prevailed during the airborne mea-

surements are not perfectly similar to the climatological means calculated by the GCM. Further, the MOZAIC data presented in Fig. 7 is only a cloud-cleared subset of all available data, and the GCM simulations may not yet cover all details of real cloud formation processes.

We stress that it is difficult to accurately determine the location of the cut-off in the GCM simulations, as subgrid-scale cloud nucleation is parameterized and not calculated explicitly as in the trajectory simulations. Because in most cases the total number of ice particles (mostly exceeding the APSC out-of-cloud criterion $n_i < 10^{-3} \text{ cm}^{-3}$) is generated within one time step, and the time step is rather large (30 min), differences between the onset RHI and the maximum RHI achieved during a freezing event cannot be resolved. For this reason, ECHAM uses as the out-of-cloud criterion $n_i = 0$. Also, RHI is computed every 12 hours from the ECHAM output of H_2O mixing ratio and T after time integration. This includes the possibility that high RHI values are built up in between, with artificially high values of RHI to be removed in the next time step by freezing and ice particle growth. Therefore, we understand that the “cut-offs” predicted by ECHAM (around 165–170 %, see Fig. 7) may lie close to the actual peak values.

We like to add that the version of Spitfire used in the present study differs from the one used in Lohmann and Kärcher (2002), which unfortunately cannot be repeated. Therefore, the cause of the difference between the simulation SPITF discussed above and the simulation TRANSP in Lohmann and Kärcher (2002) (their Fig. 9) can only be guessed. Very likely, Lohmann and Kärcher did not use a properly coded Spitfire version as their Spitfire results did not look promising.

3.4. Other data sets

In contrast to the modeled distributions shown in Fig. 7, the MOZAIC data set does not exhibit a cut-off, because relative humidities over ice exceeding 150 % have been ignored in the measurement analysis owing to the difficulty to separate cloud-free and cloudy cases properly (Klaus Gierens, personal communication, 2002). Even if such high values of RHI were considered, it would be difficult to derive specific conclusions

Relative humidity and cirrus cloud formation

W. Haag et al.

Title Page

Abstract

Introduction

Conclusions

References

Tables

Figures

◀

▶

◀

▶

Back

Close

Full Screen / Esc

Print Version

Interactive Discussion

**Relative humidity and
cirrus cloud
formation**W. Haag et al.

[Title Page](#)[Abstract](#)[Introduction](#)[Conclusions](#)[References](#)[Tables](#)[Figures](#)[◀](#)[▶](#)[◀](#)[▶](#)[Back](#)[Close](#)[Full Screen / Esc](#)[Print Version](#)[Interactive Discussion](#)

© EGU 2003

about freezing thresholds and freezing mechanisms from the full set of MOZAIC data, as we have done using the INCA data set. The MOZAIC data are long-term (three year) averages taken in a rather large spatial area. This likely averages out signatures of even significantly different individual freezing thresholds and renders inferences about individual freezing mechanisms almost impossible as very many of them may contribute to the overall distribution. In any case, it may be concluded that a freezing threshold lower than for MOZAIC is found during the INCA NH campaign, probably because the air masses over Prestwick were substantially more polluted (affected by effective IN) than those probed during the MOZAIC flights.

The distributions of RHI derived from satellite-borne measurements of the Microwave Limb Sounder (MLS) at the 215 hPa level do not exhibit cut-offs at high values (in excess of 180 %) of RHI (Spichtinger et al., 2002), while we argue that a cut-off must be present due to ice formation processes becoming active above a certain freezing threshold. We offer two explanations to solve this apparent discrepancy, bearing in mind the large field of view (FOV) of the instrument (vertical resolution: ~ 3 km, horizontal resolution $\sim 100 \times 200$ km²) and its inability to detect ice crystals smaller than about 100 μ m in size which causes retrieved RHI values to be higher than the actual RHI values in the presence of such crystals.

First, cirrus clouds could form locally and randomly in the MLS FOV and could lead to local ice saturation. If the volume of air containing ice-saturated regions is small compared to the volume probed by the MLS, the retrieved RHI signal would not be affected by the presence of cloud. Second, widespread subvisible cirrus, as those prevailing in the upper tropical troposphere, may contain only a small number of ice crystals (order 0.01 cm⁻³ or less) insufficient to drive the ice supersaturation to zero during the cloud lifetime which may be limited by sedimentation (Kärcher, 2002). This would cause high retrieved RHI values, even if the thin clouds would fill most of the volume probed by the MLS.

4. Conclusions

We summarize the following main points:

1. The slope of the probability distribution of relative humidity above ice saturation taken close to, put outside of, cirrus clouds is primarily determined by atmospheric transport (vertical motion). Cirrus cloud formation and persistence increases the slope indirectly by reducing supersaturation in regions that would otherwise remain cloud-free.

2. The cut-off of RHI distributions outside of cirrus at high relative humidities is determined by the onset of freezing of cirrus ice particles, indicating a feasible method to infer freezing threshold relative humidities of cirrus from atmospheric measurements of relative humidity.

3. The comparison between cut-off relative humidities outside of cirrus and the peak relative humidities inside cirrus is a useful tool to infer details of freezing mechanisms in cirrus clouds in cases where the difference between cut-off and peak values are larger than the experimental uncertainty.

4. The onset of freezing in clean and polluted regions of the northern hemisphere during INCA occurred at relative humidities over ice significantly lower ($\sim 130\%$) than required for homogeneous freezing ($\sim 155\%$), suggesting that the northern hemisphere background aerosol exhibits signatures of pollution in terms of cirrus formation.

5. The onset of freezing in the relatively clean southern hemisphere during INCA is consistent with homogeneous freezing, although this does not necessarily imply that only pure liquid particles were involved in cloud formation. The freezing mechanisms at work during INCA have likely involved competition between different types of freezing nuclei, especially in the northern hemisphere, and have been largely controlled by small-scale wave dynamical forcings producing a wide range of cooling rates.

6. The onset of freezing of cirrus ice particles is found to be insensitive to variations in the total number densities of condensation nuclei and accumulation mode particles. The most likely cause for the observed difference in freezing thresholds between the

Relative humidity and cirrus cloud formation

W. Haag et al.

Title Page

Abstract

Introduction

Conclusions

References

Tables

Figures

◀

▶

◀

▶

Back

Close

Full Screen / Esc

Print Version

Interactive Discussion

**Relative humidity and
cirrus cloud
formation**W. Haag et al.

[Title Page](#)[Abstract](#)[Introduction](#)[Conclusions](#)[References](#)[Tables](#)[Figures](#)[⏪](#)[⏩](#)[◀](#)[▶](#)[Back](#)[Close](#)[Full Screen / Esc](#)[Print Version](#)[Interactive Discussion](#)

© EGU 2003

two data sets are differences in chemical or morphological particle properties.

Only dedicated, short-term field campaigns carried out in a limited area, ideally characterized by uniform sources of aerosol acting as freezing nuclei, allow a meaningful interpretation of RHI distributions, provided (i) enough RHI data points (order 1,000 or more above ice saturation) have been taken and (ii) the data have enough variability in temperature. An advantage of our proposed method to infer details of freezing processes is that a Lagrangian approach to probe the clouds is not required. Lagrangian measurements are difficult to perform with aircraft, even in stationary wave clouds.

Large differences (outside the range of the experimental uncertainty in measurements of relative humidity at cirrus levels) between cut-off relative humidities outside of cirrus and the peak relative humidities inside cirrus suggest that freezing mechanisms are complex and likely involve mixtures of freezing particles with different concentrations and freezing properties, at least in the polluted northern hemisphere probed during INCA. We intend to study this in more detail in future work using the information from cirrus residual particle analyses provided by Seifert et al. (2002).

We hope that the results and inferences of this work help to improve the representation of cirrus clouds in large-scale models, along with a proper simulation of relative humidity above ice saturation. This is important in the context of atmospheric chemistry, where cirrus clouds may scavenge and vertically redistribute aerosols and reactive trace gases (such as HNO_3 or HO_2) and trigger heterogeneous chemical reactions, as well as in the context of numerical weather prediction, where the replacement of saturation adjustment schemes by a physically-based parameterization of cirrus formation would help to improve important aspects of the radiation balance and the hydrological cycle.

Acknowledgements. We thank S. Eckhardt for processing the ECMWF data used for the trajectory calculations. This research was conducted within the projects “Particles in the Upper Troposphere and Lower Stratosphere and Their Role in the Climate System” (PARTS) and “Inter-hemispheric Differences in Cirrus Properties From Anthropogenic Emissions” (INCA), funded by the European Commission and contributes to the project “Particles and Cirrus Clouds” (PAZI) supported by the Helmholtz-Gemeinschaft Deutscher Forschungszentren (HGF). U. Lohmann

is grateful for support from the project "Modelling of Global Chemistry for Climate" funded by the National Science and Engineering Research Council of Canada and the Canadian Foundation for Climate and Atmospheric Science.

References

- 5 Borrmann, S., Solomon, S., Dye, J. E., and Luo, B.: The potential of cirrus clouds for heterogeneous chlorine activation, *Geophys. Res. Lett.*, 23, 2133–2136, 1996. [3269](#)
- Braham, R. R.: Cirrus cloud seeding as a trigger for storm development, *J. Atmos. Sci.*, 24, 311–312, 1967. [3269](#)
- Danielsen, E. F.: A dehydration mechanism for the stratosphere, *Geophys. Res. Lett.*, 9, 605–608, 1982. [3269](#)
- 10 DeMott, P. J., Rogers, D. C., and Kreidenweis, S. M.: The susceptibility of ice formation in upper tropospheric clouds to insoluble aerosol components, *J. Geophys. Res.*, 102, 19 575–19 584, 1997.
- Dessler, A. E., Minschwaner, K., Weinstock, E. M., Hints, E. J., Anderson, J. G., and Russell, III, J. M.: The effects of tropical cirrus clouds on the abundance of lower stratospheric ozone, *J. Atmos. Chem.*, 23, 209–220, 1996. [3269](#)
- 15 Gattelman, A., Holton, J. R., and Douglass, A. R.: Simulations of water vapor in the lower stratosphere and upper troposphere, *J. Geophys. Res.*, 105, 9003–9023, 2000. [3271](#)
- Gierens, K. M., Schumann, U., Helten, M., Smit, H., and Marengo, A.: A distribution law for relative humidity in the upper troposphere and lower stratosphere derived from three years of MOZAIC measurements, *Ann. Geophys.*, 17, 1218–1226, 1999. [3270](#), [3285](#)
- 20 Haag, W., Kärcher, B., Schaefer, S., Stetzer, O., Möhler, O., Schurath, U., Krämer, M., and Schiller, C.: Numerical simulations of homogeneous freezing processes in the aerosol chamber AIDA, *Atmos. Chem. Phys.*, 3, 195–210, 2003. [3272](#), [3281](#)
- 25 Heymsfield, A. J. and Miloshevich, L. M.: Relative humidity and temperature influences on cirrus formation and evolution: Observations from wave clouds and FIRE II, *J. Atmos. Sci.*, 52, 4302–4326, 1995. [3269](#)
- Heymsfield, A. J., Miloshevich, L. M., Twohy, C., Sachse, G., and Oltmans, S.: Upper-tropospheric relative humidity observations and implications for cirrus ice nucleation, *Geophys. Res. Lett.*, 25, 1343–1346, 1998. [3269](#)
- 30

Relative humidity and cirrus cloud formation

W. Haag et al.

Title Page

Abstract

Introduction

Conclusions

References

Tables

Figures

◀

▶

◀

▶

Back

Close

Full Screen / Esc

Print Version

Interactive Discussion

**Relative humidity and
cirrus cloud
formation**

W. Haag et al.

[Title Page](#)[Abstract](#)[Introduction](#)[Conclusions](#)[References](#)[Tables](#)[Figures](#)[◀](#)[▶](#)[◀](#)[▶](#)[Back](#)[Close](#)[Full Screen / Esc](#)[Print Version](#)[Interactive Discussion](#)

© EGU 2003

Jensen, E. J., Toon, O. B., Pfister, L., and Selkirk, H. B.: Dehydration of the upper troposphere and lower stratosphere by subvisible cirrus clouds near the tropical tropopause, *Geophys. Res. Lett.*, 23, 825–828, 1996. [3269](#)

Jensen, E. J., Toon, O. B., Vay, S. A., Ovarlez, J., May, R., Bui, P., Twohy, C. H., Gandrud, B., Pueschel, R. F., and Schumann, U.: Prevalence of ice-supersaturated regions in the upper troposphere: Implications for optically thin ice cloud formation, *J. Geophys. Res.*, 106, 17 253–17 266, 2001. [3270](#)

Kärcher, B.: Properties of subvisible cirrus clouds formed by homogeneous freezing, *Atmos. Chem. Phys.*, 2, 161–170, 2002. [3287](#)

Kärcher, B. and Solomon, S.: On the composition and optical extinction of particles in the tropopause region, *J. Geophys. Res.*, 104, 27 441–27 459, 1999. [3270](#)

Kärcher, B. and Lohmann, U.: A parameterization of cirrus cloud formation: Heterogeneous freezing, *J. Geophys. Res.*, 108, doi:10.1029/2002JD003220, in press, 2003. [3272](#), [3283](#)

Kärcher, B. and Ström, J.: The roles of dynamical variability and aerosols in cirrus cloud formation, *Atmos. Chem. Phys. Discuss.*, 3, 1415–1451, 2003. [3268](#), [3271](#), [3282](#), [3283](#), [3284](#)

Koop, T., Luo, B. P., Tsias, A., and Peter, Th.: Water activity as the determinant for homogeneous ice nucleation in aqueous solutions, *Nature*, 406, 611–614, 2000. [3272](#), [3276](#)

Lohmann, U. and Kärcher, B.: First interactive simulations of cirrus clouds formed by homogeneous freezing in the ECHAM GCM, *J. Geophys. Res.*, 107, 4105, doi:10.1029/2001JD000767, 2002. [3284](#), [3286](#)

Lohmann, U., Kärcher, B., and Timmreck, C.: Impact of the Mt. Pinatubo eruption on cirrus clouds formed by homogeneous freezing in the ECHAM GCM, *J. Geophys. Res.*, 108, 10.1029/2002JD003185, in press, 2003. [3284](#)

Marti, J. and Mauersberger, K.: A survey and new measurements of ice vapor pressure at temperatures between 170 and 250 K, *Geophys. Res. Lett.*, 20, 363–366, 1993. [3272](#)

Minikin, A., Petzold, A., Ström, J., Krejci, R., Seifert, M., van Velthoven, P., Schlager, H., and Schumann, U.: Aircraft observations of the upper tropospheric fine particle aerosol in the northern and southern hemispheres at midlatitudes, *Geophys. Res. Lett.*, 30, doi:10.1029/2002GL016458, in press, 2003. [3280](#), [3284](#)

Ovarlez, J., Gayet, J.-F., Gierens, K., Ström, J., Ovarlez, H., Auriol, F., Busen, R., and Schumann, U.: Water vapour measurements inside cirrus clouds in Northern and Southern hemispheres during INCA, *Geophys. Res. Lett.*, 29, 1813, doi:10.1029/2001GL014440, 2002. [3277](#), [3278](#), [3281](#)

**Relative humidity and
cirrus cloud
formation**W. Haag et al.

[Title Page](#)[Abstract](#)[Introduction](#)[Conclusions](#)[References](#)[Tables](#)[Figures](#)[I◀](#)[▶I](#)[◀](#)[▶](#)[Back](#)[Close](#)[Full Screen / Esc](#)[Print Version](#)[Interactive Discussion](#)

© EGU 2003

Rasch, P. J. and Williamson, D. L.: Computational aspects of moisture transport in global models of the atmosphere, Q. J. R. Meteorol. Soc., 116, 1071–1090, 1990. [3284](#)

Rasch, P. J. and Lawrence, M.: Recent development in transport methods at NCAR, in MPI Workshop on Conservative Transport Schemes, edited by B. Machenhauer, Report No. 265, pp. 65–75, Hamburg, Germany, Max-Planck-Institute for Meteorology, 1998. [3285](#)

Seifert, M., Ström, J., Krejci, R., Minikin, A., Petzold, A., Gayet, J.-F., Schumann, U., and Ovarlez, J.: In situ observations of aerosol particles remaining from evaporated cirrus crystals: Comparing clean and polluted air masses, Atmos. Chem. Phys. Discuss., 2, 1599–1633, 2002. [3283](#), [3289](#)

Spang, R., Eidmann, G., Riese, M., Offermann, D., Preusse, P., Pfister, L., and Wang, P.-H.: CRISTA observations of cirrus clouds around the tropopause, J. Geophys. Res., 107, 8174, doi:10.1029/2001JD000698, 2002. [3270](#)

Spichtinger, P., Gierens, K., and Read, W.: The statistical distribution law of relative humidity in the global tropopause region, Meteorol. Z., 11, 83–88, 2002. [3287](#)

Stohl, A. and Seibert, P.: Accuracy of trajectories as determined from the conservation of meteorological tracers, Q. J. R. Meteorol. Soc., 124, 1465–1484, 1998. [3271](#)

Relative humidity and
cirrus cloud
formation

W. Haag et al.

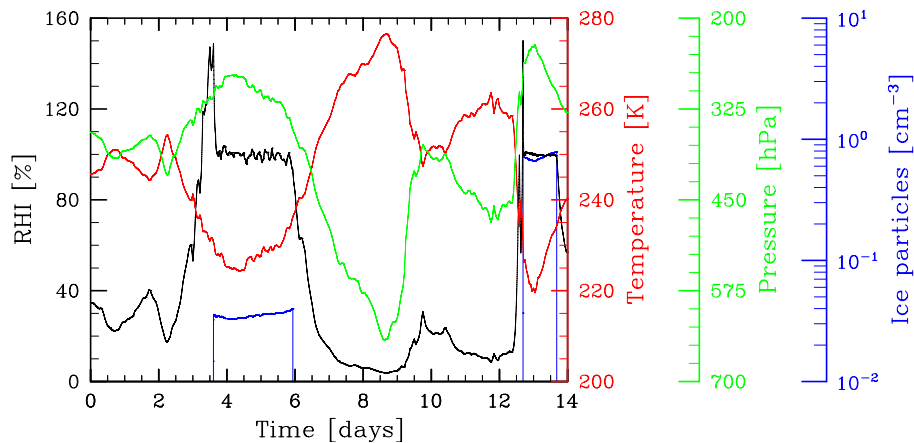


Fig. 1. Microphysical simulation along a selected trajectory showing RHI, T , p , and n_i as a function of time. See text for details.

[Title Page](#)[Abstract](#)[Introduction](#)[Conclusions](#)[References](#)[Tables](#)[Figures](#)[◀](#)[▶](#)[◀](#)[▶](#)[Back](#)[Close](#)[Full Screen / Esc](#)[Print Version](#)[Interactive Discussion](#)

© EGU 2003

Relative humidity and
cirrus cloud
formation

W. Haag et al.

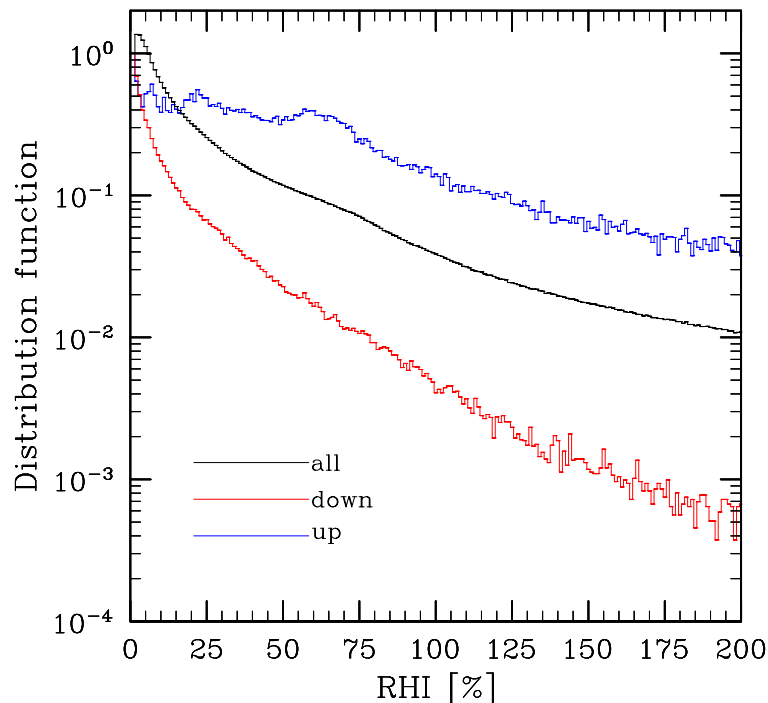


Fig. 2. Distribution of RHI calculated along atmospheric trajectories derived from high resolution ECMWF wind fields. Cloud microphysics is not included, and the RHI only varies according to changes of T and p forced by advection, while initial H_2O mixing ratios are kept fixed. The black curve represents the RHI distribution summed over all trajectories. The blue distribution results from a subset of trajectories representing net upward motion from low altitudes. The red distribution results from yet another subset representing net downward motion from the tropopause region. The RHI values were binned into 1 % intervals. All distributions are normalized with the respective number of data points in the 1 % bin (black curve: 745,086, blue curve: 1,997, red curve: 37,355).

[Title Page](#)[Abstract](#)[Introduction](#)[Conclusions](#)[References](#)[Tables](#)[Figures](#)[◀](#)[▶](#)[◀](#)[▶](#)[Back](#)[Close](#)[Full Screen / Esc](#)[Print Version](#)[Interactive Discussion](#)

Relative humidity and
cirrus cloud
formation

W. Haag et al.

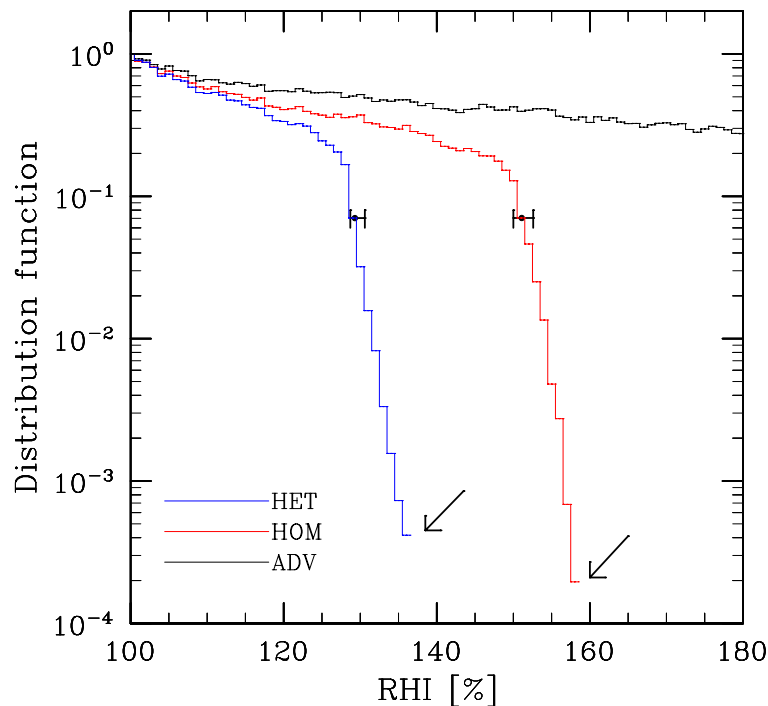


Fig. 3. Distribution of RHI outside of cirrus clouds in the layer 150–300 hPa derived from FLEX-TRA/APSC simulation including homogeneous freezing (red curve) or heterogeneous freezing (blue curve), together with the RHI distribution generated without cirrus formation (advection only, black curve). The error bars indicate the median RHIs at the onset of freezing and the corresponding first and third quartiles. The arrows define the cut-off RHIs. The RHI values were binned into 1% intervals. All distributions are normalized with the respective number of data points in the 100% bin (ADV: 12,533; HOM: 10,065, HET: 9,345).

[Title Page](#)[Abstract](#)[Introduction](#)[Conclusions](#)[References](#)[Tables](#)[Figures](#)[◀](#)[▶](#)[◀](#)[▶](#)[Back](#)[Close](#)[Full Screen / Esc](#)[Print Version](#)[Interactive Discussion](#)

© EGU 2003

**Relative humidity and
cirrus cloud
formation**

W. Haag et al.

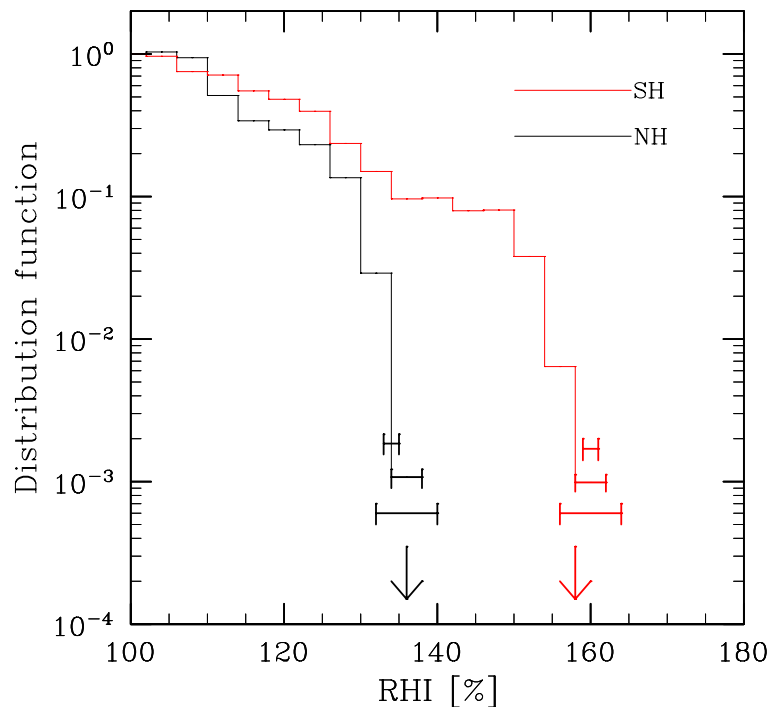


Fig. 4. Distribution of RHI above ice saturation outside of cirrus clouds measured during INCA in Punta Arenas (SH, red curve) and in Prestwick (NH, black curve). All RHI values were binned into 4 % intervals. The horizontal bars depict the range of cut-offs when using 2 % (upper bars), 4 % (middle bars), and 8 % (lower bars) intervals. The arrows mark the cut-offs derived from the modeled distributions, compare Fig. 3. The experimental uncertainty of RHI is $\pm 3\%$ (1σ -limits). The distributions are normalized with the number of data points in the 100 % bin (SH: 2,026, NH: 930).

[Title Page](#)[Abstract](#)[Introduction](#)[Conclusions](#)[References](#)[Tables](#)[Figures](#)[◀](#)[▶](#)[◀](#)[▶](#)[Back](#)[Close](#)[Full Screen / Esc](#)[Print Version](#)[Interactive Discussion](#)

© EGU 2003

**Relative humidity and
cirrus cloud
formation**

W. Haag et al.

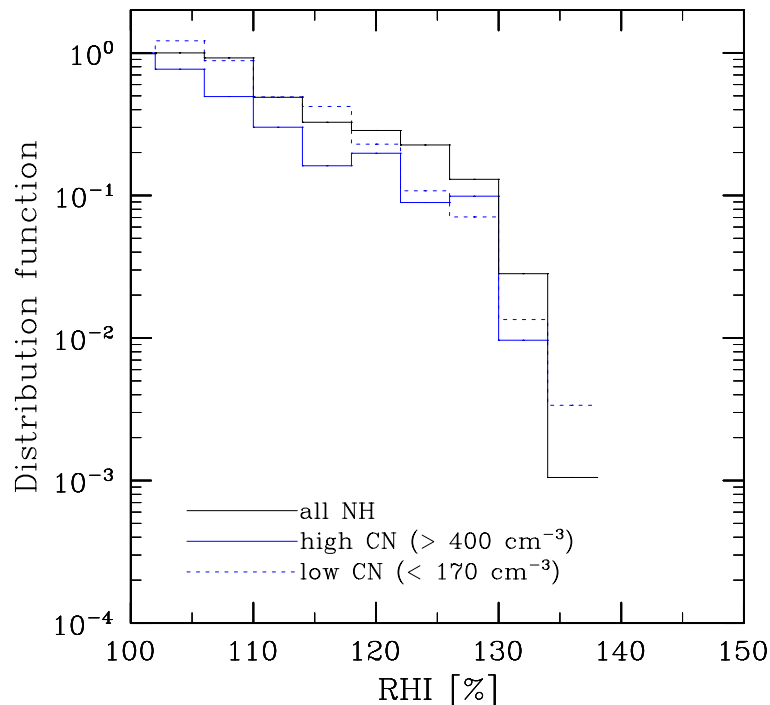


Fig. 5. Distribution of RHI above ice saturation outside of cirrus clouds measured during INCA in Prestwick (NH, black curve, repeated from Fig. 4). The solid (dotted) blue curves represent subsets of these data, representing relatively clean (polluted) airmasses with low (high) concentrations of condensation nuclei (CN) larger than 14 nm in diameter. All RHI values were binned into 4 % intervals. The CN concentrations in the clean NH case are similar to the typical CN concentrations observed in the SH. The distributions are normalized with the number of data points in the 100 % bin (NH: 930, low CN: 297, high CN: 415).

[Title Page](#)[Abstract](#)[Introduction](#)[Conclusions](#)[References](#)[Tables](#)[Figures](#)[◀](#)[▶](#)[◀](#)[▶](#)[Back](#)[Close](#)[Full Screen / Esc](#)[Print Version](#)[Interactive Discussion](#)

© EGU 2003

**Relative humidity and
cirrus cloud
formation**

W. Haag et al.

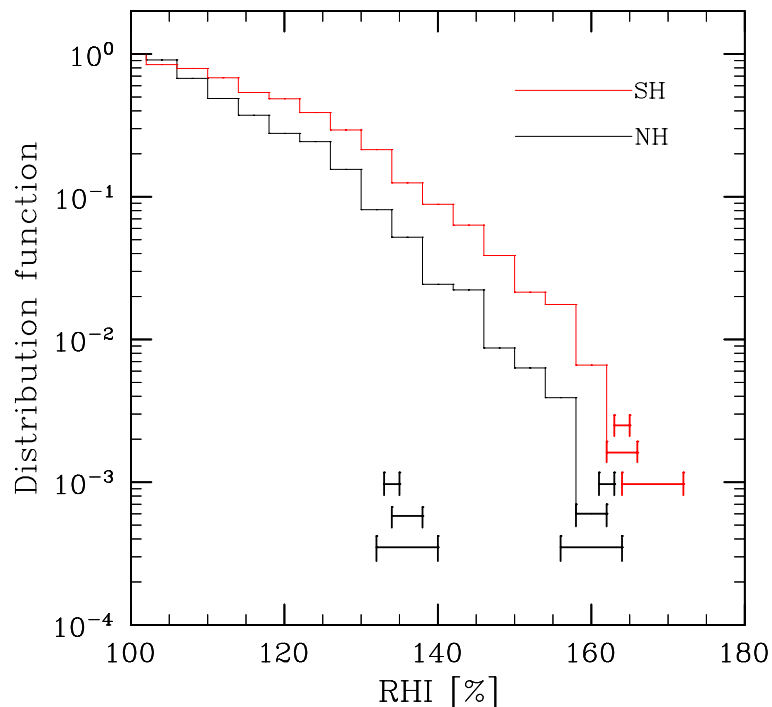


Fig. 6. Distribution of RHI above ice saturation inside cirrus clouds measured during INCA. All RHI values were binned into 4% intervals. The horizontal bars depict the range of cut-offs when using 2% (upper bars), 4% (middle bars), and 8% (lower bars) intervals. The group of bars centered above 135% are the cut-offs outside of clouds in the NH from Fig. 4, plotted here to compare with the NH in-cloud data. The experimental uncertainty of RHI is $\pm 3\%$ (1σ -limits). The distributions are normalized with the number of data points in the 100% bin (SH: 6,196, NH: 3,325)

[Title Page](#)[Abstract](#)[Introduction](#)[Conclusions](#)[References](#)[Tables](#)[Figures](#)[◀](#)[▶](#)[◀](#)[▶](#)[Back](#)[Close](#)[Full Screen / Esc](#)[Print Version](#)[Interactive Discussion](#)

© EGU 2003

**Relative humidity and
cirrus cloud
formation**

W. Haag et al.

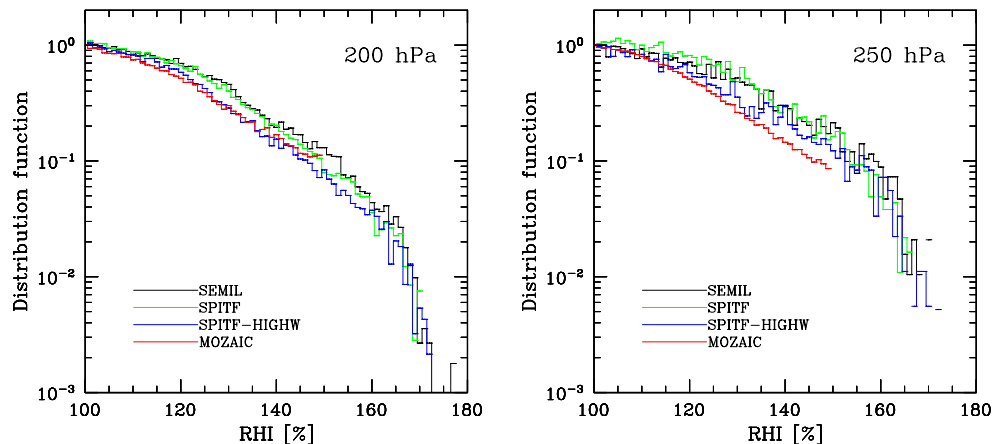


Fig. 7. Distribution of RHI above ice saturation outside of cirrus clouds derived from MOZAIC data and from ECHAM simulations (SEMIL, SPITF, SPITF-HIGHW). Both observed (in the years 1995–1997) and modeled distributions are representative for the North Atlantic region at 200 hPa (left panel) and 250 hPa (right panel). No data points above 150% have been considered in the MOZAIC data. See text for details.

[Title Page](#)[Abstract](#)[Introduction](#)[Conclusions](#)[References](#)[Tables](#)[Figures](#)[◀](#)[▶](#)[◀](#)[▶](#)[Back](#)[Close](#)[Full Screen / Esc](#)[Print Version](#)[Interactive Discussion](#)

© EGU 2003